Increasing risk of mass human heat mortality if historical weather patterns recur

Christopher W. Callahan[1,*], Jared Trok[1], Andrew J. Wilson[2], Carlos F. Gould[3], Sam Heft-Neal[2], Noah S. Diffenbaugh[1], & Marshall Burke[1,2,4]

[1]Doerr School of Sustainability, Stanford University

[2]Center on Food Security and the Environment, Stanford University

[3]School of Public Health, University of California San Diego

[4]National Bureau of Economic Research

∗Corresponding author: christophercallahan@stanford.edu

The potential death toll of severe extreme heat events is crucial for climate risk analysis and adaptation planning but may not be captured by existing projections. We estimate this quantity for Europe using machine learning to calculate the intensity of historical heat waves if they occur at present or future global temperatures, combined with empirical exposure-response functions to quantify the resulting mortality. Each event is projected to generate tens of thousands of excess deaths. If August 2003 meteorological conditions recur at the current global temperature anomaly of 1.5 °C, we project 17,800 excess deaths across Europe in one week, rising to 32,000 at 3 °C. This mortality is comparable to peak COVID-19 mortality in Europe and is not substantially reduced by ongoing climate adaptation. Our results suggest that while mitigating further global warming can reduce heat mortality, mass mortality events remain plausible at near-future temperatures despite current adaptations to heat.

This is a non-peer-reviewed preprint submitted to EarthArXiv. It has been revised and resubmitted to a peer-reviewed journal, but has yet to be formally accepted. Subsequent versions of the manuscript may differ. If accepted, the final version of this manuscript will be available via the "Peer-reviewed Publication DOI" link on the right-hand-side of this webpage.

Climate change is increasing the frequency and magnitude of extreme heat events[1–4], threatening human health[5]. Additional warming is projected to generate more intense heat events than even recent record-breaking events[6], with the potential for mass mortality events similar to those witnessed in Europe in the summer of 2003[7], especially during exceptionally hot years such as 2023[8,9].

Projections of increased heat-related mortality from climate change are now numerous[10–15]. However, these projections generally focus on the long-term population burden of non-optimal temperatures rather than the death toll of individual high-impact events. Exceptional extreme heat events require distinct management strategies compared to typical population burdens, as they can strain health and emergency services beyond what occurs at milder temperatures[16]. Preparedness for hospital overcrowding and health system surge capacity should therefore be benchmarked to a plausible extreme scenario rather than an average projection[17].

Quantifying plausible scenarios of extreme events under future climate change requires careful methodological treatment, and there are reasons to believe that existing projections do not capture the most extreme mortality events. In particular, the relatively short records of observations and global climate models (GCMs) make it difficult to assess the probabilities of the most extreme events[18]. While progress has been made using large initial-condition ensembles to quantify very rare heat mortality[19], some of the most extreme events may be poorly captured even by ensembles with many members[20]. Additionally, GCMs underestimate trends in the frequency and persistence of atmospheric circulation patterns that have contributed to recent rapid warming of heat extremes in populous regions such as Europe[21–26].

To complement existing work, a promising approach is to develop "storylines" of heat waves that are physically plausible and dynamically consistent. This conditional approach, which emphasizes plausibility rather than probability[27], enables exploration of extreme outcomes[28,29] and stress-tests of adaptation strategies[17,30]. Plausible storylines must also account for the documented ability of humans to adapt to repeated heat exposure, and to change behavior following past extreme heat episodes[31].

Major heat mortality events require multiple ingredients: large-scale physical drivers

of elevated temperatures as well as human health responses to the resulting heat stress. Extreme heat events tend to occur when atmospheric high-pressure systems interact with dry soils to produce land-atmosphere feedbacks that amplify heat accumulation[6,21,32,33]. In turn, prolonged exposure to high ambient temperatures impairs the body's ability to dissipate heat, leading to elevated core temperature, increased cardiovascular strain, and a heightened risk of heat-related illness and death[34].

Here, we focus on the combination of these geophysical and physiological ingredients in Europe. Hot extremes are increasing more rapidly in Europe than the rest of the hemisphere[22,23,26], and tens of thousands of deaths across the continent have been linked to recent summer heat[35,36], with climate change causing more than half[37]. As a result, Europe is a particularly timely setting in which to study the risk of mass heat mortality events.

We combine two existing approaches to quantify the risk of mass heat mortality across Europe (Methods). First, we use a recently developed machine learning framework[38]. In this framework, convolutional neural networks are trained on an ensemble of GCMs from the sixth phase of the Coupled Model Intercomparison Project (CMIP6) to predict daily temperatures in three IPCC regions of Europe from the annual global mean temperature (GMT), calendar day, and modeled daily meteorological conditions; then, meteorological conditions from ERA5 reanalysis are used as out-of-sample inputs to the trained neural networks to predict "counterfactual" versions of historical heat waves at varying annual GMT. Our method learns the GCMs' representation of the meteorological drivers of individual extreme heat events, allowing us to quantify the intensity of surface temperature extremes conditional on historical meteorological patterns, independent of projected changes in the frequency or persistence of those patterns. We predict counterfactual events at varying annual GMT, rather than long-term mean GMT, because individual hot years are plausible before long-term climate targets are reached[39] and pose significant regional climate risks[40].

For this study, we produce counterfactual estimates of five multi-week periods of extreme heat that occurred in July 1994, August 2003, July 2006, June 2019, and August 2023. While these illustrative events had differing durations and spatial extents, we

choose them because each corresponds to a continuous period of Europe-wide temperature anomalies (date ranges shown in Fig. S1), shows spatial patterns of anomalous atmospheric pressure and soil moisture (Fig. 1g), and spans a wide range of human influence on the climate (e.g., annual GMT anomaly of 0.6 °C in 1994 vs. 1.5 °C in 2023).

Second, we use longitudinal data on temperature and weekly mortality over 2015-2019 from 924 subnational regions of Europe to estimate exposure-response functions that relate ambient temperature to mortality risk (Methods). We control for location-specific seasonal and trending factors, isolating plausibly exogenous variation in temperature to measure the causal effect of temperature on mortality. We then calculate mortality from each event at each GMT anomaly and compare it to a long-term average baseline without global warming. We estimate and propagate uncertainty throughout the calculation, resulting in mortality projections that incorporate variation in both the counterfactual event predictions and exposure-response function (Methods).

These tools allow us to explicitly separate the effects of climate change and weather variability on mortality. We can leverage the diverse library of weather patterns simulated by GCMs to learn nonlinear relationships between meteorological patterns and surface heat extremes, along with the heterogeneity of responses to global warming across those patterns[38]. Whereas previous studies of climate change and mortality in Europe have been limited to linear scaling to capture multiple events[37] or computationally intensive custom simulations for an individual event[41], our approach allows us to leverage an ensemble of CMIP6 simulations to predict temperature profiles resulting from different historical meteorological conditions at different annual GMTs. In this way, our out-of-sample application of these learned relationships to actual meteorological patterns grounds our analysis in weather systems that have historically produced extreme heat.

Results

After training on GCMs, our machine learning predictions compare well with summer daily temperatures in ERA5 across Europe when using ERA5 meteorological fields as out-of-sample inputs (Fig. 1a-c; out-of-sample $R^2 \geq 0.92$ across regions). They also

specifically predict variation in the temperature of the hottest week in each region (Fig. 1d-f; out-of-sample $R^2 \geq 0.85$). We observe a small cold bias in Northern Europe (Fig. 1f), potentially because the most extreme days in the GCM training data are slightly cooler than the tail of the ERA5 distribution in this region (Fig. S2). In the construction of counterfactual events, we use a "delta" method that bias-corrects the predictions (Methods). Finally, we find close correspondence between predicted and true temperatures when evaluating on held-out GCM data across a wide range of annual GMT anomalies (Fig. S3, out-of-sample $R^2 \geq 0.98$).

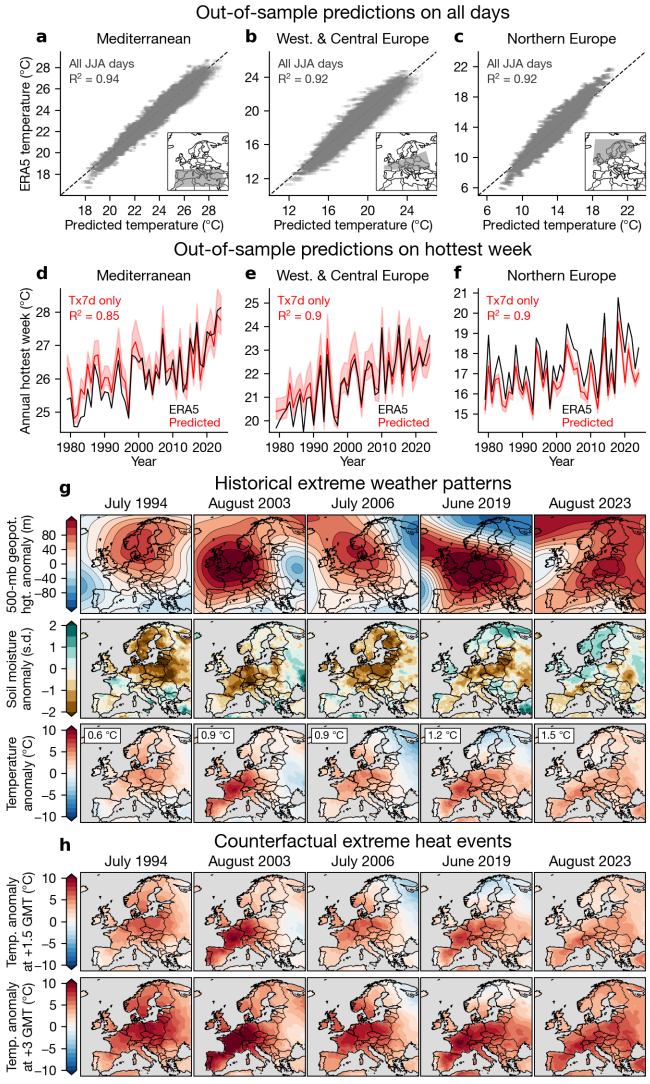

Figure 1: Using machine learning to quantify historical and counterfactual heat waves in Europe. a-c) Daily mean temperatures in June, July, and August (JJA) in our out-of-sample machine learning predictions and ERA5 reanalysis, for the IPCC regions of the Mediterranean (a), Western and Central Europe (b), and Northern Europe (c). Inset maps show region definitions. d-f) Time series of annual hottest 7 days (Tx7d) from ERA5 (black) and out-of-sample predictions (red) over the same regions. Red line shows the mean prediction and shading shows 95% confidence interval across GCMs and random seeds used in training (Methods). g) Meteorological conditions during five selected extreme heat events, with 500-mb geopotential height in top row, soil moisture in middle row, and temperature in bottom row. Inset text in bottom row denotes the annual GMT anomaly (vs. 1850-1900) in the corresponding year. h) Counterfactual temperature anomalies during each of the five heat waves at annual GMT anomalies of 1.5 and 3 °C. Meteorological anomalies are relative to the location and day-of-year mean over 1979-2023 and averaged over the days defined for each event (Fig. S1).

Together, these results indicate that our approach is capable of closely reproducing sequences of hot days at a range of annual GMT values when provided with particular historical meteorological patterns, despite not seeing those precise patterns in training.

Turning to our illustrative heat waves, while the weather patterns associated with each event vary, they share common characteristics: anomalous high-pressure systems and dry soils across the continent, resulting in elevated temperatures in many countries (Fig. 1g). Without global warming, each event would have been cooler (Fig. S4); likewise, with additional warming, a given meteorological pattern produces steadily higher temperature anomalies (Fig. 1h, Fig. S4). The difference between the actual event magnitude and the magnitude at different annual GMT varies by event, both because the actual events occurred at different GMT and because the machine learning approach learns different responses to global warming conditioned on the particular meteorological pattern[38]. Across annual GMT of 1.5, 2, 3, and 4 °C, the August 2003 conditions yield the highest temperatures of all events, emphasizing the severity of the weather conditions during that event (Fig. 1h, Fig. S4). Similarly, July 1994, for which temperature anomalies were relatively moderate among the illustrative events, produces among the most severe anomalies at standardized GMTs.

High temperatures are empirically associated with increased mortality risk across Europe (Fig. 2). We specifically find that the heat-mortality relationship is moderated by a region's long-term mean temperature, as found elsewhere[11]; for example, the minimum mortality temperature (MMT) is 14.5 °C in the coolest third of regions and 19.7 °C in the warmest third of regions. This heterogeneity may reflect the greater return on adaptation investments such as air conditioning in warmer regions. However, the slope of the exposure-response curve is steeper for warmer areas despite their higher MMT, potentially reflecting limits to adaptation to the hottest conditions. For all regions, the nonlinear increase in mortality risk above the MMT means that greater extreme heat intensity is expected to increase mortality across the continent (Fig. 2, lower inset points).

Each extreme heat event is projected to generate thousands of weekly excess deaths across Europe at the current annual GMT of 1.5 °C[42], with increasing impacts in response to higher GMT (Fig. 3, Table S1). The largest death tolls are associated with the 1994 and

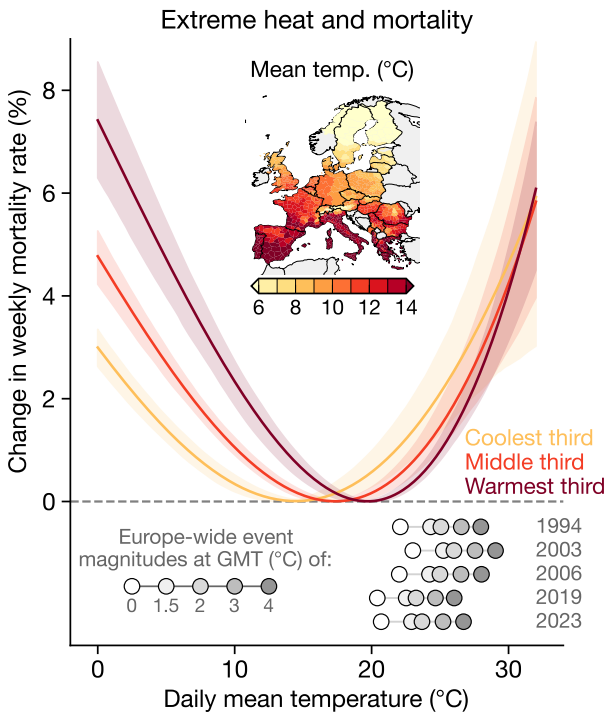

Figure 2: Temperature-mortality relationship across Europe. Relationship between daily temperatures and change in cumulative weekly mortality rate in subnational regions across Europe over 2015-2019, as a function of regions' mean temperature (computed over 2000-2019). Curves show examples for the coolest third (yellow), middle third (orange), and warmest third (red) of regions. Effects are accumulated across the contemporaneous week and the following three weeks by including three lags in the regression (Methods). Map shows mean temperature for each region for which we have mortality data. Lower inset points show the population-weighted Europe-wide average temperature during each event at a range of annual GMTs above the pre-industrial baseline.

2003 conditions, with 26,500 (95% confidence interval [CI]: 22,400 - 31,100) and 32,000 (CI: 26,700 - 38,800) weekly excess deaths in a 3 °C year, respectively (Fig. 3a, b). While less likely than more moderate temperatures given current emissions trends, individual years at 4 °C are still plausible under gradual decarbonization[40] and would generate 37,500 (CI: 29,500 - 46,400) and 45,100 (CI: 37,000 - 55,600) excess deaths in a single week across Europe if 1994 or 2003 meteorological conditions recurred, respectively. The other three events are associated with weekly peaks of 25,600 (CI: 21,000 - 30,700), 18,800 (CI: 16,100 - 22,100), and 20,900 (CI: 16,700 - 25,800) excess deaths, respectively, at 3 °C. Excess mortality is slightly negative in the weeks following the event, consistent with mortality displacement (Methods), though not enough to offset the peak of the event.

These death tolls reflect the underlying effect of hot temperatures without climate change, combined with the influence of climate change in intensifying these events. Comparing each event to its counterfactual at 0 °C allows us to isolate the contribution of climate change to event mortality (red lines vs. gray shading in Fig. 3). For example, at the peak of a 2003-like event at 3 °C, we project climate change to produce an additional 23,000 excess deaths on top of 9,000 that would have occurred without warming, making

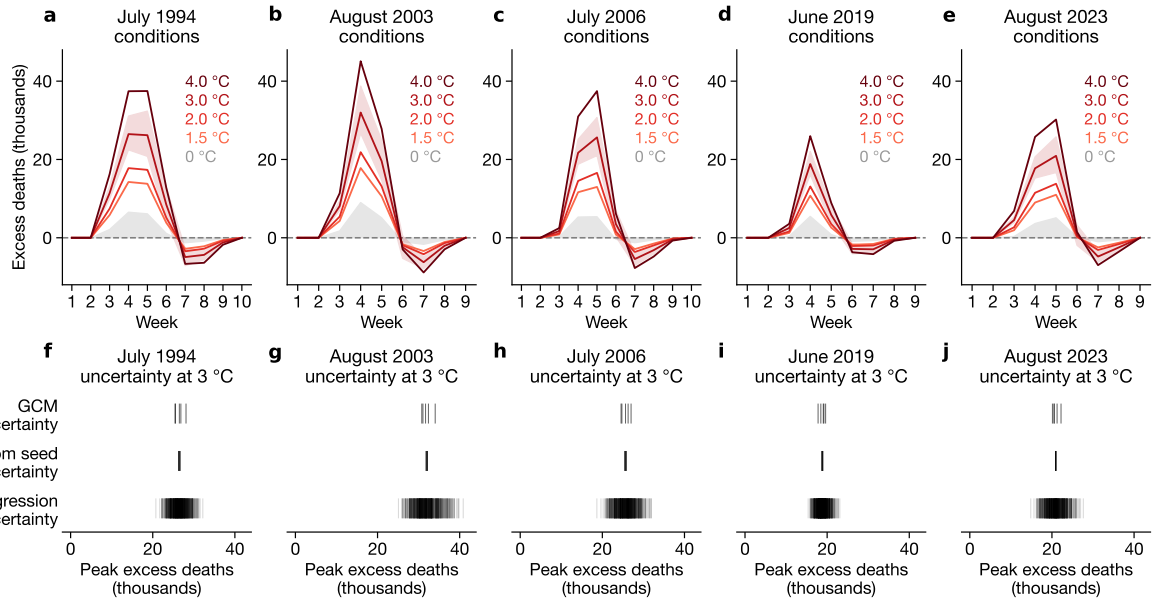

Figure 3: Mortality during counterfactual extreme heat events. Top row shows Europe-wide weekly excess mortality during extreme heat events based on meteorological conditions from July 1994 (a), August 2003 (b), July 2006 (c), June 2019 (d), and August 2023 (e) across a range of annual global temperatures. Solid line shows average projection and shading shows 95% range in a year with GMT 3 °C above the pre-industrial baseline. Gray shading shows mortality at 0 °C, meaning the mortality that would have occurred without global warming. The x-axis spans two weeks before the event begins to three weeks after it ends to illustrate the lagged effects of the event on mortality (Methods). Bottom row shows sources of uncertainty in the peak death toll from the July 1994 (f), August 2003 (g), July 2006 (h), June 2019 (i), and August 2023 (j) events. For each uncertainty source, the other dimensions are held at their average values and lines show variation across each value of the relevant dimension.

anthropogenic warming responsible for 72% of the death toll (Table S2).

Uncertainty in mortality from each event (shading in Fig. 3a-e) results from differences across GCMs used for machine learning training, uncertainty in the machine learning training process, and sampling uncertainty in the exposure-response function (Methods). Examining the contribution of each source of uncertainty while holding the others constant reveals that sampling uncertainty in the exposure-response function ("regression uncertainty") is the dominant source across all five illustrative events (Fig. 3f-j). While the GCMs we use for training do not span the full CMIP6 ensemble (Methods), our subset does include both high- and low-sensitivity GCMs. The higher-sensitivity GCMs have lower mortality projections than the lower-sensitivity GCMs (Fig. S5), mak-

ing it unlikely that global climate sensitivity is the primary driver of GCM uncertainty in the mortality response to increasing GMT.

The spatial distribution of mortality during each event differs, governed by the location of temperature anomalies (Fig. 1), variation in exposure-response functions (Fig. 2), and spatial variation in the effect of global warming (Fig. S6). For example, under 1994-like conditions, the greatest mortality occurs in Germany, Poland, and Eastern Europe, whereas under 2023-like conditions, mortality is highest in Spain, Italy, and the Balkans (Fig. S7).

Given that European countries undertook adaptation to heat following previous events such as 2003[31], and we observe heterogeneity in exposure-response functions that may indicate adaptation (Fig. 2), we explore the potential for additional future adaptation to mitigate mortality from these events. Specifically, we allow each region's mean temperature to evolve in the future according to pattern scaling coefficients derived from CMIP6 GCMs (Fig. S8, S9), and adjust the exposure-response function accordingly (Methods). Following other work[11], our approach to estimating adaptation thus relies on extrapolating current heterogeneity in exposure-response functions and assumes that future societies will continue to adapt with the same pattern as has been recently observed.

Across the five illustrative events we study, incorporating adaptation reduces peak mortality by only 10% on average (Fig. 4). For example, peak mortality during 2003 meteorological conditions in a 3 °C year is projected to be 31,900 in our main projections and 28,800 (CI: 21,300 - 36,200) when allowing additional adaptation. The with-adaptation peak mortality from the 2003 event remains larger even than the no-adaptation peak of the other events. These results imply that there is limited potential for currently deployed adaptation approaches to reduce the mortality impacts of these extreme climate events.

Discussion

Several caveats and analytical choices should be considered when evaluating these results. For instance, we use all-age mortality rather than age-stratified rates to maximize

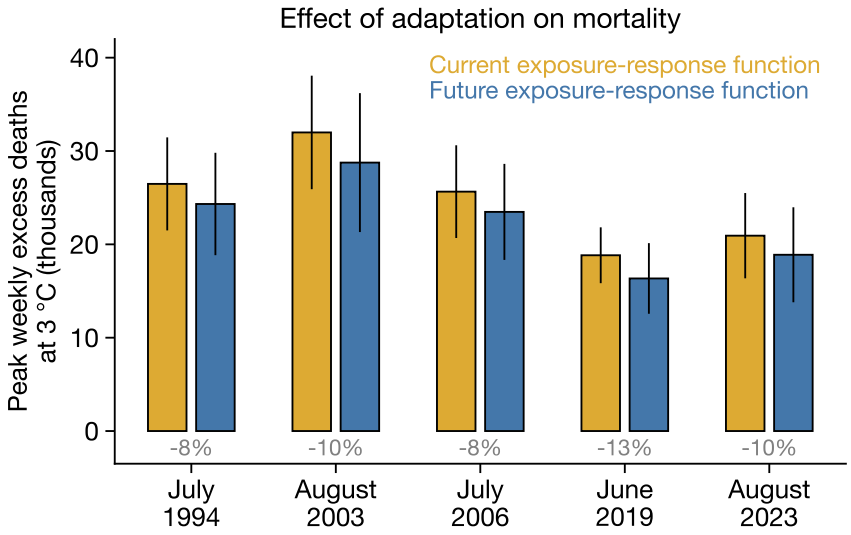

Figure 4: Limited potential to reduce heat mortality by scaling up observed adaptation. Each bar shows the peak weekly mortality at 3 °C for each set of meteorological conditions. The yellow bars show our main calculation (i.e., the peak of the 3 °C curve in Fig. 3), which incorporates existing adaptation through spatial heterogeneity in exposure-response functions. The blue bars show the same calculation after accounting for additional future climate adaptation by allowing exposure-response curves to evolve with future climate change (Methods). Bar heights shows average projections and error bars show 95% range. Gray text denotes the percent reduction in mortality from additional future adaptation.

data coverage (Methods), meaning we do not account for future shifts in age structure. However, we find an extremely similar exposure-response function for the over-65 population as for all ages (Fig. S10), meaning that our main response is likely already driven primarily by mortality among the elderly. Additionally, previous work has projected that changes in age structure are likely to increase heat-related mortality in Europe by 1-3%, implying that they would only slightly affect our results[43].

Our use of annual GMT as a predictor differs from other work defining global warming as a multi-decade smoothed value[44]. Our goal is to quantify the mortality risks associated with the possibility that historical meteorological conditions recur in years that are globally hotter than the historical years in which those conditions occurred. While smoothed GMT isolates long-term global warming, realized climate risks reflect the combination of the forced response and internal variability, and individual extreme years such as 2023 have seen dangerous local heat conditions as a result of this combina-

tion[8,9]. As a result, quantifying the intensity of plausible heat waves at specific annual GMTs provides critical information for risk assessment.

Additionally, our projections are conditional on weather patterns that are rare by definition. It is possible that these mortality events would not take place even with substantial warming if the corresponding meteorological conditions do not occur again. Conversely, even more severe events could be produced if weather patterns occur that were not witnessed in the short observational record. Further, our results reveal a latent potential for meteorological patterns that did not cause significant excess mortality in the past to do so in the future if they occur at higher GMTs. For example, at equivalent GMT, the July 1994 meteorological conditions produce the highest cumulative mortality and second highest peak mortality of any of the illustrative events (Table S1).

This finding also illustrates the reason that we avoid calculating "observed" mortality from each event at the time it actually occurred. Each event occurred at a different level of warming and potentially a different degree of human adaptation to heat. Indeed, in other recent work, we show that the heat-mortality relationship in France is very different before 2003, meaning that calculating "observed" heat mortality in 2003 may require a more sophisticated exposure-response function[45]. Our forward-looking approach allows us to analyze a range of known meteorological conditions at the same GMT levels, permitting standardized comparisons between historically different events with a single exposure-response function that reflects recent adaptation.

To further contextualize the magnitude of the death tolls we calculate, we compare them to weekly confirmed COVID-19 deaths across the same regions of Europe for which we have mortality data (Fig. 2, inset map). For example, the most severe 10% of weeks of COVID-19 had between 27,900 and 34,100 confirmed deaths. At 3 °C, the weekly death toll from 2003-like conditions is comparable to these peak weeks of COVID-19, and at 4 °C, the weekly death tolls of 1994-, 2003-, and 2006-like conditions would exceed even the single worst week of COVID-19 in Europe (Fig. S11).

It is notable that our results suggest limited potential for existing patterns of adaptation to mitigate these mass mortality events. This result may occur because although warmer regions in Europe have higher MMTs, they also have steeper exposure-response

curves above those MMTs (Fig. 2). However, our approach to adaptation is based solely on extrapolating observed spatial heterogeneity as a function of mean temperature. If other factors such as income change in the future, this could further affect the exposure-response function. To explore this issue, we run an additional regression where temperature is simultaneously interacted with both mean temperature and mean income[11], and we find that mean temperature generates much greater heterogeneity than income, providing confidence that our main findings capture the most important axis of heterogeneity at present (Fig. S12). More broadly, our results are consistent with other work emphasizing that heat still poses a major public health threat despite putative progress since the deadly 2003 summer[46–48], and point to the need for novel approaches to emerge if adaptation is to be more effective.

Conclusion

Our results reveal a substantial death toll from potential future extreme heat events in Europe. These results are based on historically observed meteorological patterns combined with plausible 21st-century global temperature anomalies, making them physically realistic storylines of high-magnitude heat events. We specifically distinguish between the contributions of climate change and natural variability conditional upon these realistic patterns, revealing that climate change is already a dominant contributor to mortality during extreme heat events, and its contribution could reach 70-80% of deaths at higher levels of warming.

Our characterization of specific, plausible high-magnitude outcomes is an important complement to existing heat mortality projections and can help inform health system preparedness and planning. Most importantly, our results demonstrate that even if global temperatures are stabilized, substantial and novel adaptation measures may be required to reduce the continent-wide threat of extreme heat to population health.

Methods

Data

We draw weekly mortality data from the Eurostat database (data code "demo_r_mweek3"). Different regions make data available over different time periods; we limit our analysis to 2015-2019 to match the most common period of data availability, following other work[35]. Where possible, we use all-age, all-sex mortality rates from NUTS3 (third administrative level below country) regions, except in Germany, where we only have these data at the NUTS1 level. This yields a total of 924 regions with continuous mortality rate data over 2015-2019. Age-group-specific rates (e.g., 65+) are available for only a slightly smaller number of regions (N = 908), so we use all-age rates to maximize coverage in our preferred specification.

Our historical climate data come from the E-OBS station-based dataset[49] and the ERA5 reanalysis[50]. We use E-OBS daily surface temperature when possible, including for the initial definitions of each extreme event and the mortality calculations. E-OBS data are spatially averaged to the appropriate NUTS regions, weighting grid cells within regions by the population of each grid cell. We use ERA5 for the out-of-sample machine learning predictions (Fig. 1) and maps of historical meteorological conditions (Fig. 1).

Counterfactual extreme heat events

We use a machine learning architecture recently developed and validated by Trok et al.[38] to produce counterfactual versions of historical extreme heat events. Following this approach, we train convolutional neural networks (CNNs) on an ensemble of GCM realizations, with the goal of predicting daily mean temperature anomalies over a specified region given daily meteorological conditions and the annual global mean temperature anomaly (GMT).

The predictors for each day are daily sea level pressure (SLP), daily geopotential height (GPH) fields at the 700-, 500-, and 250-mb levels, daily soil moisture (SM) between 0 and 10 cm, the calendar day, an indicator variable for each GCM, and the GMT anomaly over the previous 12 months. Prior to training, the meteorological predictors are detrended with respect to the grid cell, calendar day, and GMT, and then standardized

by subtracting the grid-cell calendar-day mean and dividing by the grid-cell calendar-day standard deviation[38]. The detrended and standardized surface pressure, geopotential height, and soil moisture are the factors we refer to as "meteorological conditions" throughout the text. Using detrended and standardized anomalies in this process means that these meteorological conditions explain day-to-day variation in temperature, but do not contain the signal of global warming. Daily mean temperature anomalies (the predictands) are referenced to the 1979-2023 period, with GMT anomalies relative to the same period when used in training. However, we note that throughout the text we refer to GMT anomalies relative to 1850-1900.

In our experimental setup, we train the CNN on a pooled set of CMIP6 simulations: three realizations each of five GCMs (CanESM5, HadGEM3-GC31-LL, MIROC6, MPI-ESM1-2-LR, and UKESM1-0-LL). We combine the historical and SSP5-8.5 simulations to create a 1850-2100 dataset for each realization. These five GCMs are chosen because they each archive three-dimensional daily atmospheric fields of each input variable from multiple realizations of the GCM. While these data requirements prevent us from using a wider range of CMIP6 models, these five GCMs are representative of the range of climate sensitivities in the CMIP6 ensemble[51]. Since this analysis focuses on summer heatwaves, we train each CNN on CMIP6 data from May through September.

We then apply the model to predict daily temperature anomalies using predictor data from ERA5. One set of predictions uses the observed GMT time series, whereas the other sets use counterfactual GMT values but maintain the other daily predictors from the reanalysis. The result is a set of counterfactual temperature time series that maintain realistic day-to-day weather conditions but vary according to the annual GMT anomaly. While we train the CNN on a pooled set of realizations, we include an indicator variable for each GCM which allows the CNN to make separate predictions based on differences between individual GCMs. This indicator variable is one-hot encoded and provided to the neural network after the convolutional layers along with the calendar-day and GMT inputs (similar to Trok et al.[38]). In training, we also vary the random seed 5 times to account for random differences in model training. This procedure yields 25 total predictions for each counterfactual event and GMT anomaly, 5 random seeds each for 5

GCMs.

We use a "delta" method to apply the CNN predictions to E-OBS gridded observations. For each day in the event of interest, we take the difference between the counterfactual CNN predictions on that day and the original CNN predictions for that day using the actual GMT. We then apply these deltas to the E-OBS observed data for that day to calculate counterfactual daily time series. Finally, we aggregate these counterfactual gridded daily temperature data into averages at the NUTS region level as with the original observations.

In Trok et al.[38], the CNNs were trained to predict temperature in regions chosen for their relevance to specific historical extremes. In our application, we would like to apply these predictions to a set of events, each with slightly different spatial footprints. We therefore train the CNNs to predict temperature change on land in each of three regions as defined by the Intergovernmental Panel on Climate Change (IPCC): the Mediterranean (MED), Western and Central Europe (WCE), and Northern Europe (NEU)[52]. The events manifest differently in each of these regions, with temperatures generally highest in the Mediterranean region and lowest in Northern Europe (Fig. S6). We then apply the deltas for each region uniformly to the grid cells within each region. When training the CNNs, the input SLP, GPH, and SM fields are defined by broader regions of approximately 35° latitude and 85° longitude centered on the IPCC regions[38].

Exposure-response functions

We use panel regression with fixed effects to measure the causal effect of temperature on mortality across Europe. This widely used approach[11,12,53–55] involves regressing mortality rates on a nonlinear function of temperature, along with vectors of intercepts (fixed effects) that non-parametrically remove seasonal or annual average factors separately for each region.

We also account for heterogeneity across regions by interacting temperature with each region's 2000-2019 average temperature, allowing the temperature exposure-response curve to vary based on a region's long-term climate. This approach leverages cross-sectional variation in temperature to assess societal adaptation to extreme heat, in effect

asking whether the same temperature level has a different effect in a region that is warmer on average than a region that is cooler on average. Cross-sectional variation is less amenable to causal identification since there may be other factors (e.g., income, demographics) that are correlated with both average temperature and heat sensitivity. Nevertheless, assessing heterogeneity by mean temperature is a well-established strategy for identifying present and future climate adaptation[11,56–59], so we adopt it here while acknowledging the potential for additional relevant axes of heterogeneity. Our approach is also similar to multi-stage methods that have been used in other recent papers to estimate variation in exposure-response functions (e.g.,[13,60,61]), though we run a single regression that accommodates variations across regions rather than pooling time series regressions from separate regions.

Specifically, we estimate the following regression relating contemporaneous and lagged temperature vectors $\mathbf{T}$ to log mortality rates M in region i, week w, and year y with Ordinary Least Squares:

$$M_{iwy} = \sum_{j=0}^{L} \left[f(\mathbf{T}_{i(w-j)y}) + f(\mathbf{T}_{i(w-j)y}) \times \overline{T}_i \right] + \mu_{iy} + \delta_{iw} + \epsilon_{iwy} \quad (1)$$

The region-year fixed effects μ_{iy} and region-week fixed effects δ_{iw} remove the influence of long-term trends and seasonal cycles that could confound the temperature-mortality relationship, and do so separately for each region. The $\overline{T}_i$ term denotes the 2000-2019 mean temperature in each region i. We estimate distributed lag models that sum the impact on mortality of contemporaneous and lagged temperature exposure, with j indexing weekly lags. As discussed below, our main model uses 3 weeks of lagged temperatures. Regressions are weighted by each region's population.

A key consideration is that mortality rates are provided at the weekly scale but temperature extremes can impact mortality rates on daily timescales. We require a strategy that preserves daily nonlinearities while matching the weekly scale of the mortality data. We thus follow previous work[11] and sum the daily mean temperature from each day d within week w after a fourth-order nonlinear transformation has been applied to each day's temperature:

$$f(\mathbf{T}_{iwy}) = \beta_1 \sum_{d=1}^{7} T_{iw(d)y} + \beta_2 \sum_{d=1}^{7} T^2_{iw(d)y} + \beta_3 \sum_{d=1}^{7} T^3_{iw(d)y} + \beta_4 \sum_{d=1}^{7} T^4_{iw(d)y} \quad (2)$$

We estimate independent coefficients for each of the summed polynomial terms in Eqn 2. Because weekly mortality rates are the sum of daily mortality rates (given constant population), calculating the effects of daily sums preserves the nonlinear effect of each individual day on weekly mortality rates. We use daily mean temperature following earlier work[11], but using daily maximum or daily minimum temperatures yields only small differences in exposure-response functions (Fig. S10).

We use lags in the regression to incorporate delayed effects of temperature. These delayed effects could arise simply due to additional mortality if people die several days after heat exposure. They could also manifest as "displacement" or "harvesting," where mortality is abnormally low after heat waves since the heat accelerated the deaths of people who would have died soon regardless of the heat. Indeed, we do observe some displacement following the events (Fig. 3), as the lag-2 and lag-3 regression coefficients are negative (Fig. S13). We use three lags in our main analysis following earlier work[35], but re-estimating the model using 6 lags yields similar results, with potentially slightly more displacement in additional weeks (Fig. S13).

Our main regression is estimated over 2015-2019, as the period over which the greatest number of regions have continuous mortality data. Alternatively, we estimate the regression using all observations from 2000-2019, though different regions have different numbers of observations over this period. We find a very similar response, though the mortality response to high temperatures is slightly stronger when including data farther back in time (Fig. S10), consistent with other evidence of moderate adaptation to heat over this period[31,48]. Because the 2015-2019 sample utilizes a balanced set of regions with continuous data and accounts for previous adaptation to heat, we use it in our main analysis.

When we test an additional interaction with income (Fig. S12), we calculate income as the 2000-2019 mean of log annual GDP per capita. GDP per capita is defined in Euros, GDP-deflated to account for inflation and purchasing-power-parity adjusted.

Calculating counterfactual mortality

Our central calculation compares a series of abnormally hot days at a given GMT level to a long-term mean baseline without global warming (Fig. S4). We perform this calculation by applying the exposure-response function (Fig. 2) to the temperature time series in each region and comparing it to the same prediction when applied to the baseline time series. Because our outcome is log mortality, the difference between each prediction yields a percent change in mortality due to experiencing the temperature at each GMT instead of the baseline temperature. We then multiply this percent change by the average number of deaths in each region observed over 2015-2019 to calculate the additional mortality from each event. Because these deaths are relative to an underlying baseline number of deaths, we refer to them as "excess deaths" or "excess mortality."

Note that we generally refer to the events predicted by the machine learning method for different GMT anomalies as "counterfactual" events, whereas we use "baseline" to refer to a long-term average without the event.

One key methodological question in this procedure is the construction of the baseline temperature from which excess deaths are calculated. We are interested in the total number of excess deaths associated with each event, not just those caused by climate change. We therefore construct a baseline which does not include either climate change or extreme heat events. This is done in two steps:

1. We use the machine learning approach described above to construct counterfactual estimates for every summer day between 1980-2023 at 0 °C. We subtract the "delta" from this procedure from the E-OBS observations to construct a counterfactual dataset at 0 °C over the entire observational time period (i.e., not just for each event). This yields a 44-year counterfactual temperature time series for each region that includes daily weather variability and extreme heat events, but not the influence of climate change.

2. We then take the long-term average across 1980-2023 from this counterfactual time series for each calendar day in each region.

The result of this calculation is an estimate of the average seasonal cycle in each

region at 0 °C. Because the influence of climate change was removed from these observed temperatures, this baseline does not include global warming, and because it was averaged over all years for each calendar day, it does not include deviations from the seasonal cycle (i.e., it does not include extreme heat events). The black dashed line in Fig. S4 shows the Europe-wide average of these baseline temperatures over the time period of each event.

Adaptation to climate change

Our regression approach (Eqn. 1) accounts for current adaptation to heat by allowing exposure-response functions to vary according to regions' 2000-2019 mean temperature. This approach assumes that vulnerability to temperature during the 2015-2019 data period fully reflects efficient levels of adaptation investment (such as installing air conditioning, taking indoor jobs rather than working outdoors, or implementing heat action plans in cities), justifiable based on longer-term (2000-2019) exposures. In the future, especially in light of rising incomes, we might expect additional such actions, which could reduce the death toll that we project.

We project future adaptation under the assumption that changes in regions' long-run mean temperatures directly translate into additional adaptation actions. We thus require an estimate of future long-run (i.e., 20-year) mean temperature in each region, with which to adjust the exposure-response functions (Fig. 2). However, our approach predicts event intensity using annual global temperature, a quantity which does not directly translate into local mean temperatures over the previous 20 years. Therefore, we adopt a pattern scaling approach, following IPCC AR6 WGI Chapter 4[62], to simulate increased 20-year mean temperatures in each European subnational district depending on a given annual GMT. We use 27 models from the sixth phase of the Coupled Model Intercomparison Project[63], spanning the historical and SSP3-7.0 experiments[64]. For each year, we calculate GMT anomalies (relative to 1850-1900) and local mean temperature anomalies over the previous 20 years for each European region (relative to 2000-2019). For example, for 2069 in the region that encompasses Berlin, we have the GMT change in 2069 and the regional mean temperature change over 2049-2068. The relationship be-

tween these two quantities yields a coherent spatial pattern across Europe (Fig. S9) that is reflective of the forced response[62]. We note that extreme temperatures in Europe are rising faster than both local and global averages, and CMIP6 models generally underestimate this higher scaling[23,24], but changes in local 20-year mean temperatures in CMIP6 models scale with GMT quite similarly to their scaling in E-OBS observations (Fig. S8).

In each calculation of event mortality at each annual GMT, we predict each region's additional mean temperature change (relative to 2000-2019) given the GMT, slope, and intercept, and add this additional temperature change to the region's 2000-2019 mean temperature. This new mean temperature value is then used in the calculation of each region's mortality from their exposure-response functions (Fig. 2), allowing the exposure-response functions to evolve in the future given a projection of changing local mean temperatures.

Finally, we implement two sensitivity tests of this adaptation approach. In the first test, we calculate analogous scaling factors from observations rather than GCMs, by regressing regional 20-year-running-mean temperature change from E-OBS against HadCRUT global mean temperature anomalies. We then assume that each region's rate of local mean warming continues linearly into the future. In the second test, we simply assume that each European region's mean temperature changes by the same amount as the GMT level (i.e., we assume a 1-to-1 scaling between global and local mean temperature). In both cases, we find effects of adaptation that are very similar to our main analysis (Fig. S14).

Uncertainty quantification

Our analysis incorporates uncertainty from each step in the calculation. First, when estimating the empirical exposure-response functions, we estimate uncertainty by bootstrap resampling 500 times (see *Exposure-response functions* section). We block-bootstrap by country, meaning we preserve temporal correlation within NUTS regions and spatial correlation across regions within countries (akin to clustering standard errors by country). Second, when making counterfactual temperature predictions for historical weather patterns using the machine learning architecture (see *Counterfactual extreme heat*

events section), we make 25 different counterfactual event predictions for each extreme heat event at each annual GMT anomaly (making a different prediction for each of 5 random seeds within each of 5 different GCMs).

We calculate each final mortality projection 12,500 times ($5 \times 5 \times 500$), once for each combination of regression bootstraps, random seeds, and GCMs. In the uncertainty decomposition in Fig. 3, we hold two dimensions of uncertainty at their mean values and show all values across the remaining dimension (e.g., each of 500 different results for each regression bootstrap while averaging across GCMs and random seeds).

When we incorporate adaptation (see *Adaptation to climate change* section), we pool all model-years and calculate a random sample of 100 pattern scaling coefficients from this pooled sample. Then, in each of the 12,500 mortality calculations, we randomly sample one of these sets of pattern scaling coefficients.

Given the multiple dimensions of uncertainty that we account for, we round each value in the main text to three significant figures to avoid reporting overly precise results.

Data and Code Availability

Replication code and data are available at: `https://zenodo.org/records/15625966`.

Author Contributions

C.W.C., N.S.D., and M.B. designed the study. C.W.C. and J.T. performed the analysis. A.J.W., C.F.G., S.H.-N., N.S.D., and M.B. provided feedback on the analysis and interpretation of results. C.W.C. wrote the first draft of the paper with all authors providing feedback.

Acknowledgements

We thank members of Stanford's Environmental Change & Human Outcomes and Climate & Earth System Dynamics groups for helpful feedback. We thank the Stanford Doerr School Center for Computation and Stanford Research Computing Center for providing computational resources that contributed to our results. We acknowledge

funding support from Stanford University.

Competing Interests

The authors declare no competing interests.

Supplementary Materials

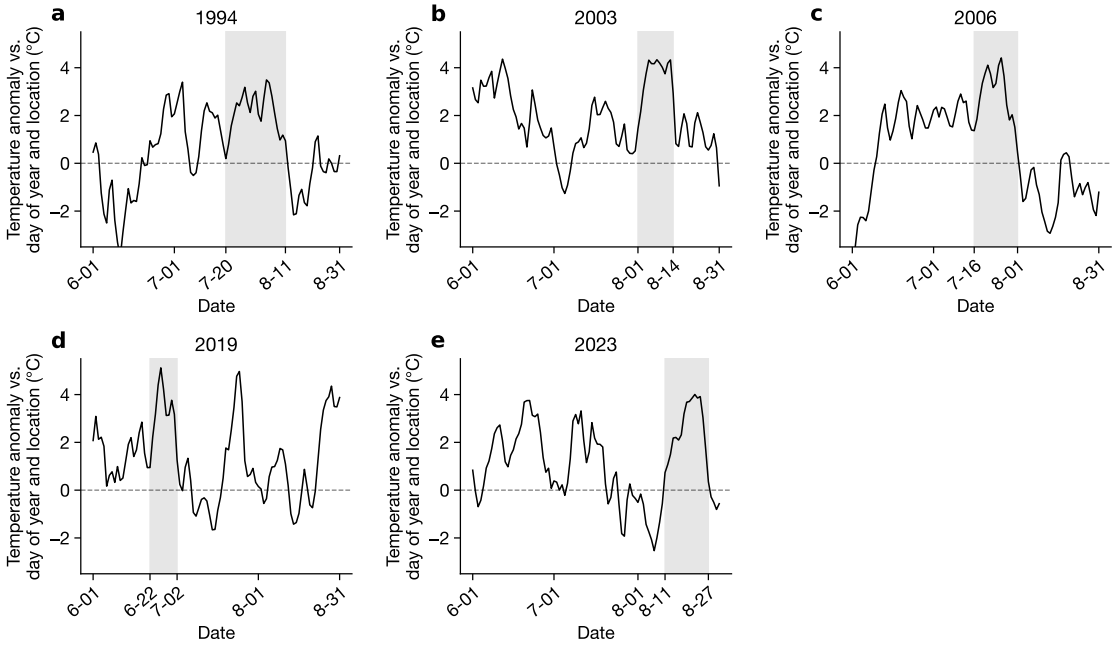

Figure S1: Temperature anomalies for selected events. Each plot shows temperatures anomalies from June through August, calculated as the population-weighted mean across all European subnational regions for which we have mortality data. Anomalies are calculated with respect to each region and day of year. Gray shading shows the periods that we define as each event. Colored lines show average counterfactuals and shading shows 95% confidence intervals across 25 combinations of GCMs and random seeds.

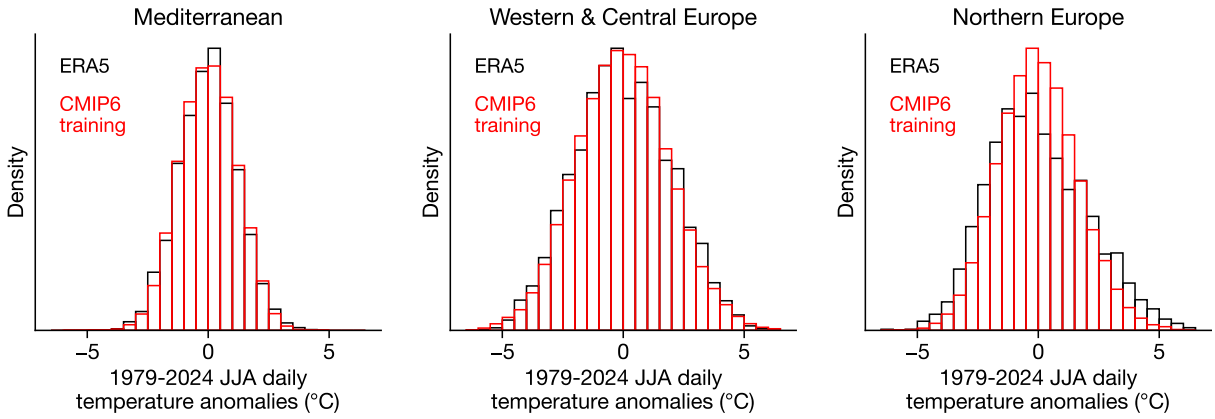

Figure S2: Temperature anomalies in each European region. Each distribution shows the range of June-July-August daily temperature anomalies (relative to day-of-year mean) in ERA5 (black) and the CMIP6 data used for machine learning training, in the three regions used in training.

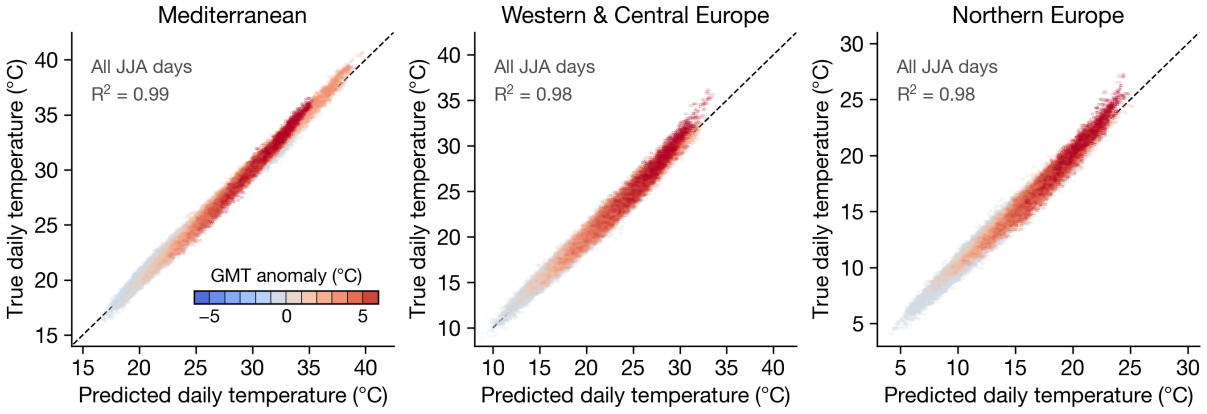

Figure S3: Machine learning predictions of unseen GCM data. Relationship between predicted values and true values simulated by GCMs, when the machine learning algorithm has been trained on a subset of GCM data and evaluated on the held-out sample.

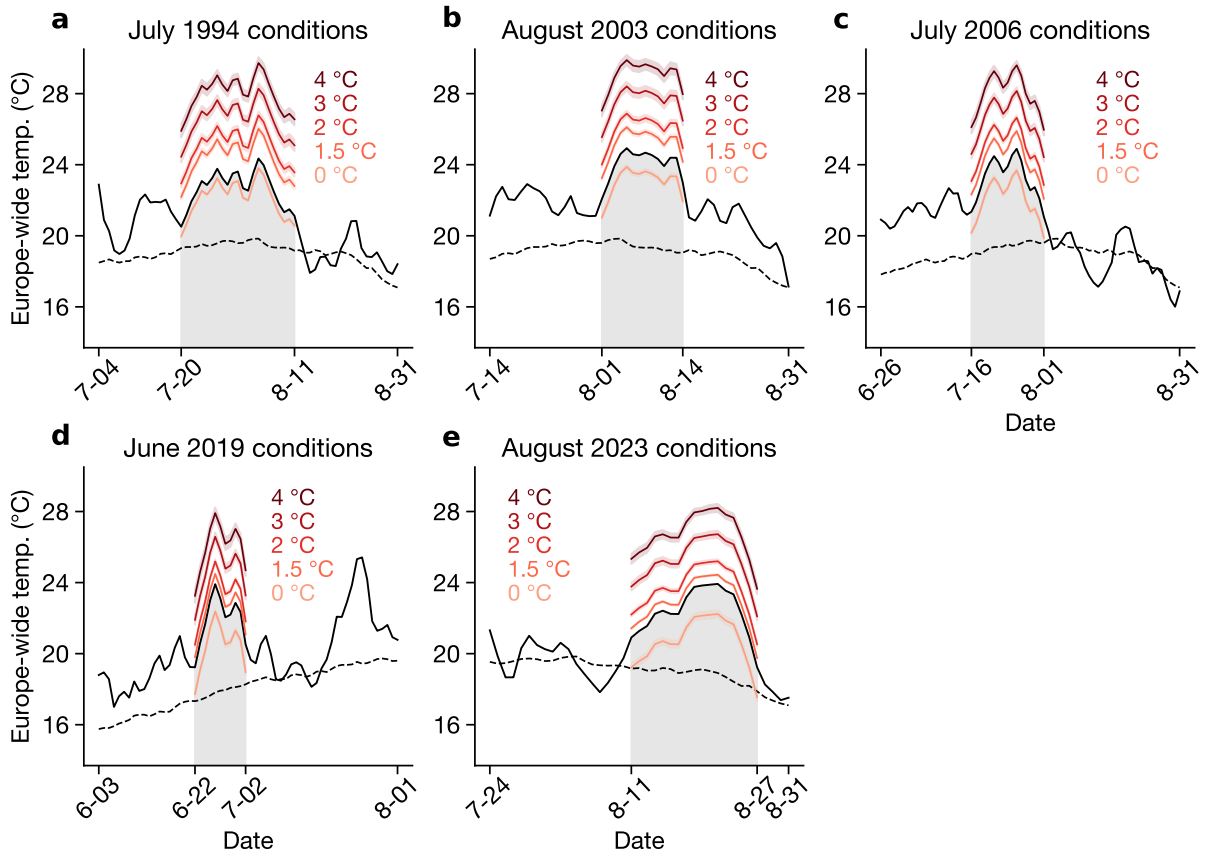

Figure S4: Actual and counterfactual Europe-wide temperatures. Time series of observed (from E-OBS; black solid line), baseline without warming or heat waves (black dashed line), and counterfactual event (red colored lines) temperatures across Europe. Europe-wide temperatures are calculated as the population-weighted average across all subnational regions for which we have temperature data. Gray shading denotes the periods we define as the "events"; these dates are originally defined using Europe-wide temperature anomalies (Fig. S1) but are shown here for clarity.

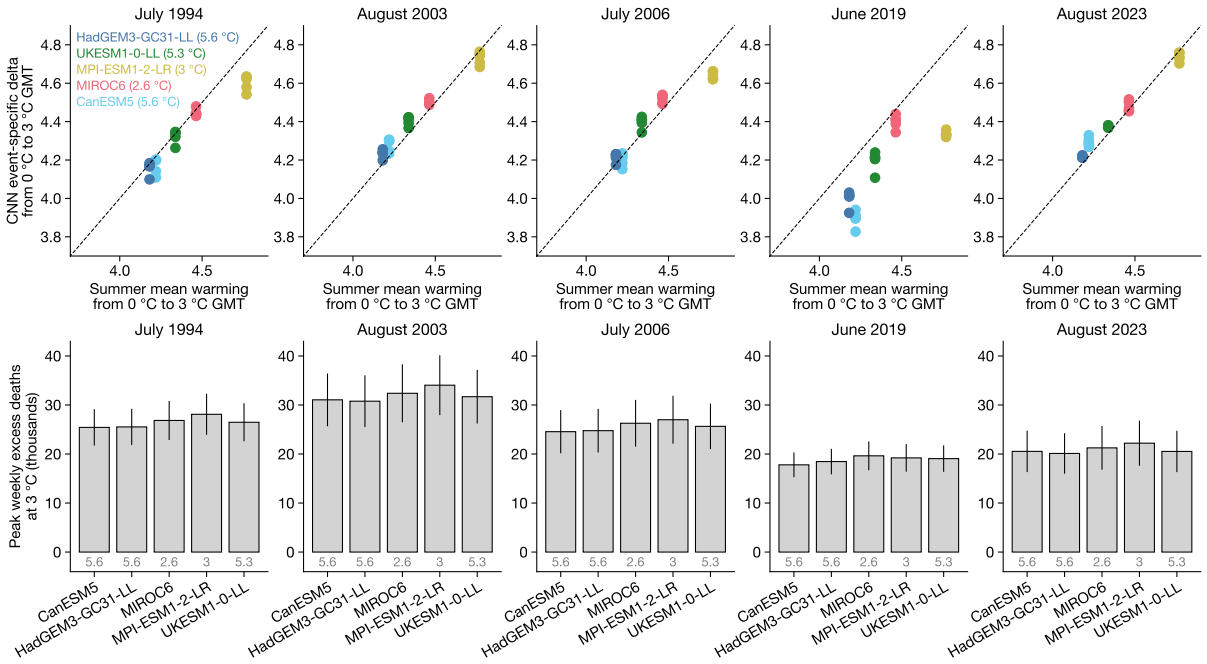

Figure S5: GCM-specific warming trends and mortality projections. Top row: Change in JJA mean temperature averaged across the three European regions from the raw GCM training data when moving from 0 to 3 °C (x-axis), plotted against the change in event intensity from 0 to 3 °C predicted by the machine learning approach (y-axis). Colors denote different GCMs, with their equilibrium climate sensitivity (ECS) noted in parentheses in the upper left panel. Different dots for a given GCM correspond to predictions using different random seeds in the machine learning training. Bottom row: Peak mortality projected for each event for annual GMT 3 °C above the pre-industrial baseline, separated according to the GCM used to train the neural network. Bar height shows average prediction and line spans the 95% confidence interval across random seeds and regression bootstraps. Lower text denotes the ECS for each GCM from Meehl et al.[51].

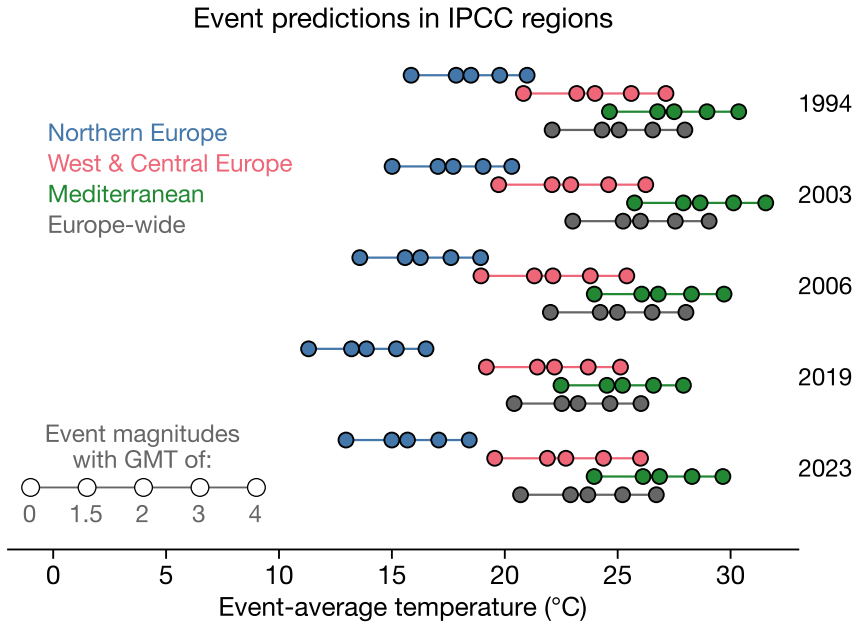

Figure S6: Temperature for each event in IPCC AR6 regions. As in the lower points in Fig. 2, but for each of the three IPCC regions for which we train the CNNs.

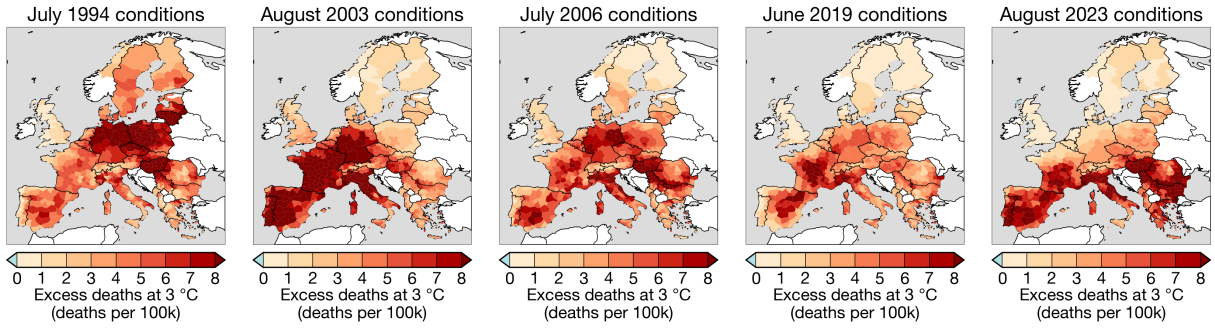

Figure S7: Regional mortality rates during extreme heat events. Each panel shows the regional mortality rate, in deaths per 100,000 population, in the peak week of each counterfactual heat wave at 3 °C. Peak weeks are defined as the week of maximum Europe-wide excess deaths (i.e., maximum point in Fig. 3). White regions are those for which we do not have population or mortality data.

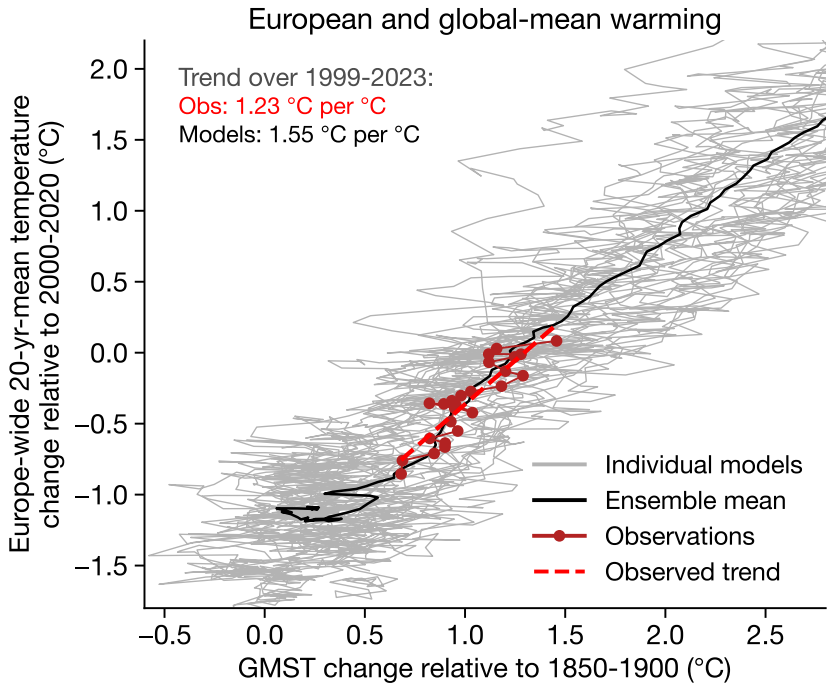

Figure S8: Observed and simulated rates of warming in Europe. Each line plots the annual global mean temperature change relative to 1850-1900 on the x-axis against 20-year running mean of Europe-wide temperature relative to 2000-2019 on the y-axis. "Europe-wide" temperature means the average across NUTS regions. 20-year running means are used because we find that the 20-year average 2000-2019 temperature of each NUTS region shapes the exposure response function in Fig. 2. Gray lines show each individual CMIP6 model, black line shows the ensemble mean, dark red line shows the E-OBS observations, and red dashed line shows a linear fit to the observations. X-axis is truncated to focus on lower warming levels to enable visual comparison between observations and models. 1999 is used as the first year of the slope calculation because using a 20-year running mean drops every previous year between 1980 and 1999.

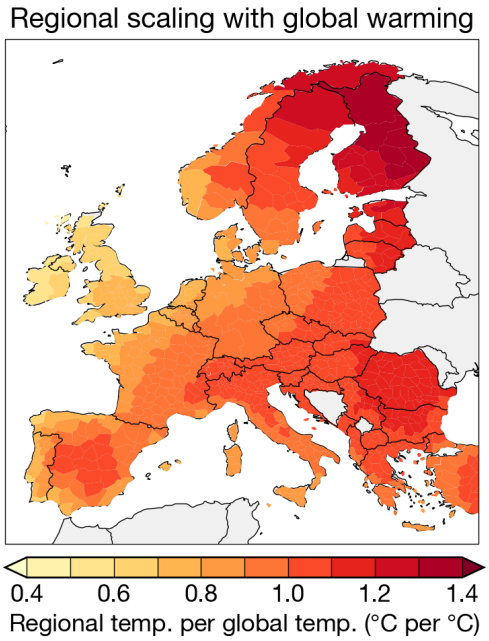

Figure S9: Pattern scaling coefficients across European regions. Linear coefficient between annual global temperature and regional mean temperature in the previous 20 years. Coefficients are averaged across 100 random samples of pooled model-year populations.

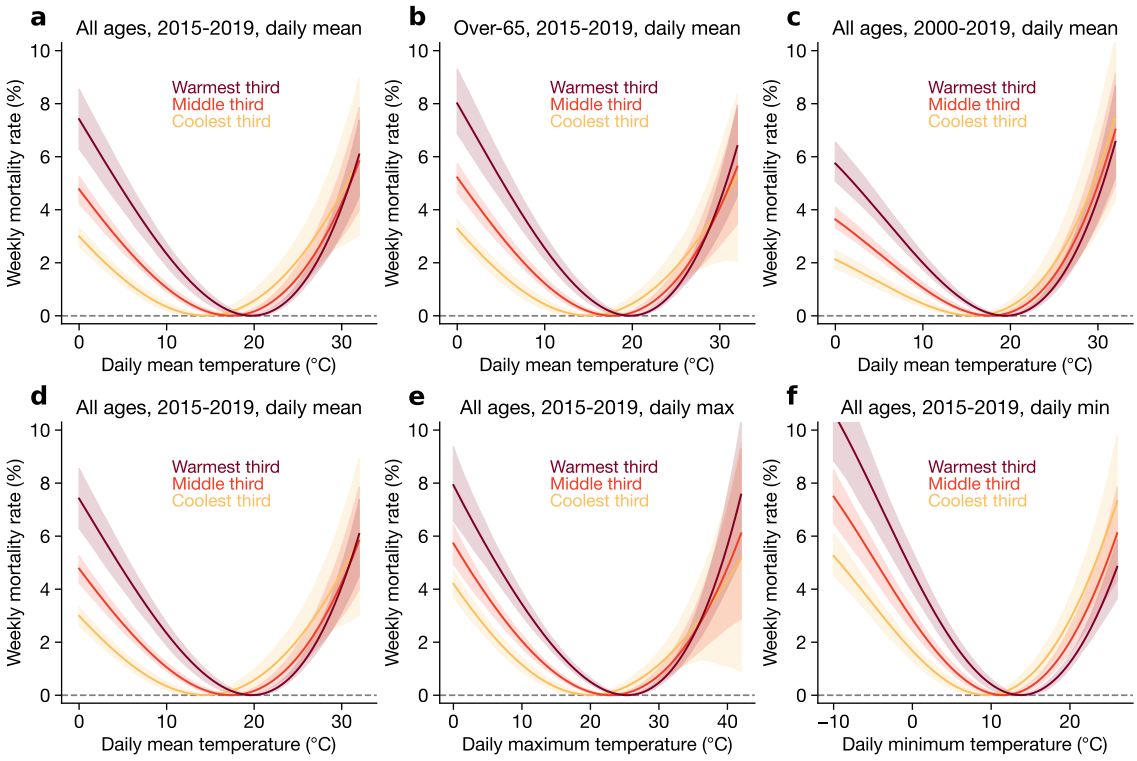

Figure S10: Alternative exposure-response curves. Panel (a) shows our main exposure-response function, which uses all-age mortality over 2015-2019 (same as Fig. 2). Panel (b) shows the same regression specification using over-65 mortality. Panel (c) shows the all-age response over 2000-2019 instead of 2015-2019. Panel (d) again shows our main exposure-response function, which uses daily mean temperature. Panels (e) and (f) show the same specification using daily maximum (e) and minimum (f) temperature. Note that the x-axes are scaled differently in (e) and (f) to account for the different observed ranges of the temperature metrics. All y-axes are standardized.

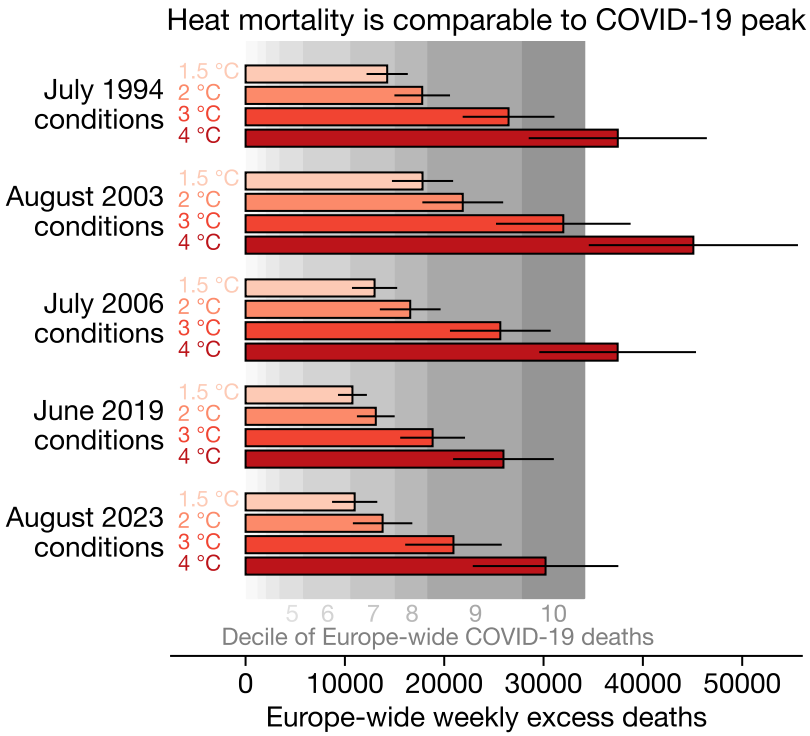

Figure S11: Peak heat mortality compared to peak COVID-19 mortality. Red bars show peak weekly mortality from each set of meteorological conditions (i.e., the peaks of the curves in Fig. 3). Bar widths show mean projection and error bars show 95% range. Gray shading shows the deciles of Europe-wide weekly confirmed COVID-19 deaths. For example, the darkest gray shading shows the range of the top 10% of weeks of COVID-19 deaths, the second-to-darkest shading shows the range of the top 10-20% of weeks, and so on.

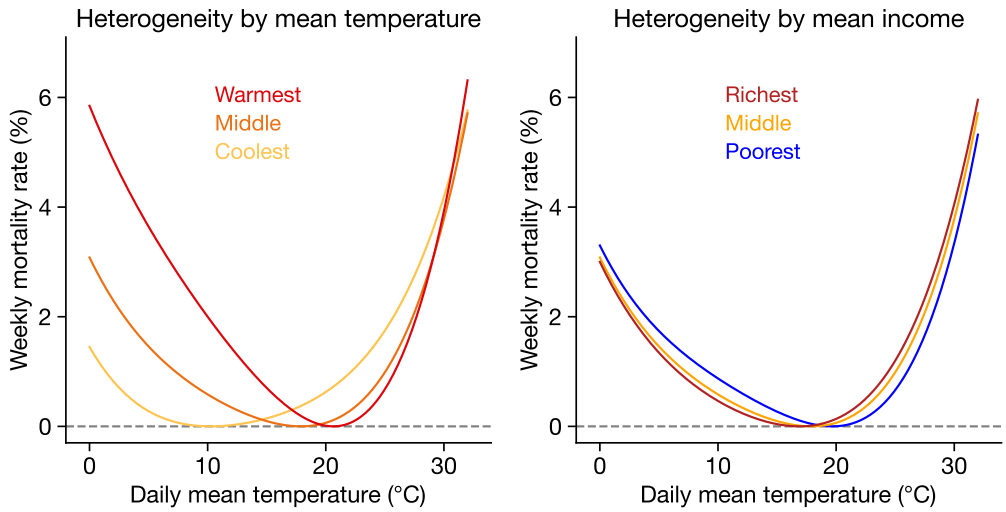

Figure S12: Heterogeneity in exposure-response function by climate and income. Both panels show results from a single regression model where the polynomials of daily mean temperature are interacted with continuous values for both a region's mean climate and its mean log income. The left panel shows responses for the coolest, middle, and warmest tercile (analogous to Fig. 2), when evaluated at the middle tercile of income. Conversely, the right panel shows the responses for the poorest, middle, and richest tercile of income, when evaluated at the middle tercile of climate.

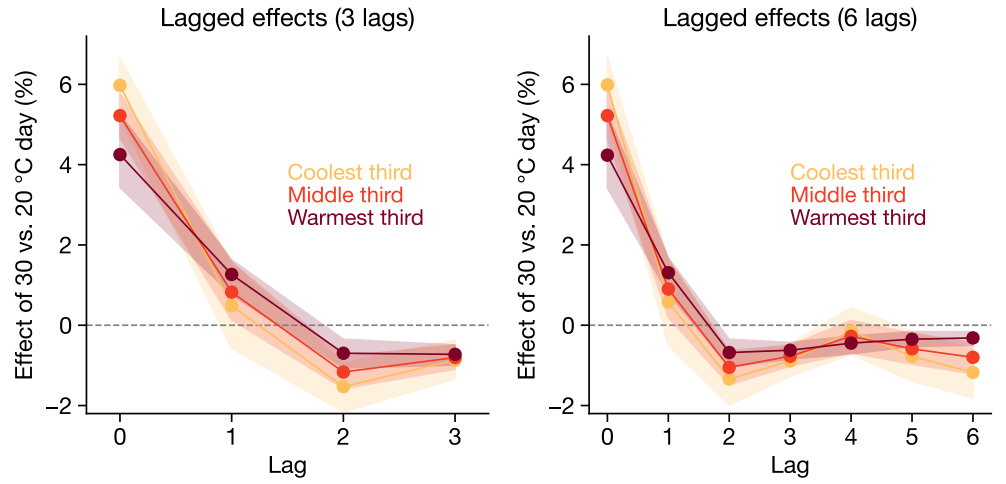

Figure S13: Effect of a hot day across lags. Both panels show the mortality effect of a 30 °C day relative to a 20 °C day, at a series of lags relative to the week of mortality. Lag 0 means contemporaneous temperature, lag 1 means temperature the week before, and so on. In our main analysis, we use 3 lags (left panel), but we also test a model with 6 lags (right panel).

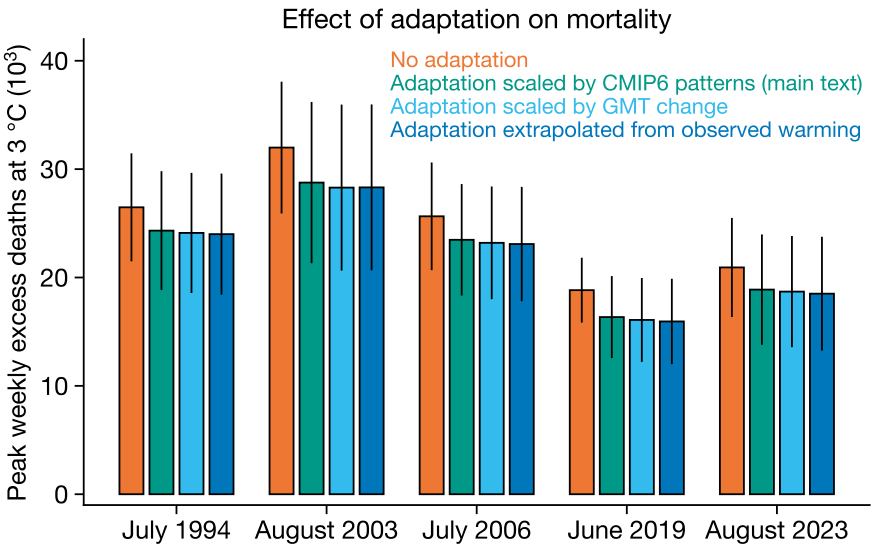

Figure S14: Alternative approaches to estimating adaptation. As in Fig. 4, but with two additional versions of adaptation. Orange bars show our main result without adaptation. Green bars show the effect of adaptation using CMIP6 pattern scaling, as in main text Fig. 4. Light blue bars show adaptation when regional 20-year-mean temperatures are assumed to scale 1-to-1 with annual GMT. Dark blue bars show adaptation when the rate of regional warming (relative to GMT change) is extrapolated linearly from observations, with the slope calculated over 1999-2023 (Fig. S8).

Event	GMT	Peak mortality	Cumulative mortality
July 1994	1.5	14300	32100
July 1994	2.0	17800	40700
July 1994	3.0	26500	62000
July 1994	4.0	37500	89100
August 2003	1.5	17800	26500
August 2003	2.0	21900	33000
August 2003	3.0	32000	48900
August 2003	4.0	45100	69500
July 2006	1.5	13000	21700
July 2006	2.0	16600	27900
July 2006	3.0	25600	43500
July 2006	4.0	37500	63800
June 2019	1.5	10800	11000
June 2019	2.0	13100	13800
June 2019	3.0	18800	20900
June 2019	4.0	26000	29800
August 2023	1.5	11000	18300
August 2023	2.0	13800	23500
August 2023	3.0	20900	36700
August 2023	4.0	30200	53800

Table S1: Europe-wide mortality for each event. Each row shows the maximum weekly excess deaths ("peak") and cumulative excess deaths for each event at each global mean temperature ("GMT"). We note that because the events differ slightly in their durations (Fig. S1), peak single-week mortality is more directly comparable across events than cumulative mortality. Values are rounded to three significant figures to avoid excessive precision given multiple dimensions of uncertainty in these calculations.

Event	GMT	Peak mortality from warming	Percent from warming
July 1994	1.5	7700	54%
July 1994	2.0	11200	63%
July 1994	3.0	20100	76%
July 1994	4.0	31300	84%
August 2003	1.5	8800	49%
August 2003	2.0	12900	59%
August 2003	3.0	23000	72%
August 2003	4.0	36100	80%
July 2006	1.5	7600	59%
July 2006	2.0	11200	67%
July 2006	3.0	20300	79%
July 2006	4.0	32100	86%
June 2019	1.5	5300	49%
June 2019	2.0	7600	58%
June 2019	3.0	13300	71%
June 2019	4.0	20500	79%
August 2023	1.5	5900	53%
August 2023	2.0	8700	63%
August 2023	3.0	15800	76%
August 2023	4.0	25100	83%

Table S2: Climate change-driven mortality for each event. The "peak mortality from climate change" row shows the peak weekly excess deaths for each event at each GMT relative to the peak of the event at 0 °C, meaning only the component of mortality due to anthropogenic intensification of the event. The "percent from warming" column shows the percent of overall peak mortality (Table S1) due to climate change. Values are rounded to three significant figures to avoid excessive precision given multiple dimensions of uncertainty in these calculations.

References

[1] Gerald A Meehl and Claudia Tebaldi. More intense, more frequent, and longer lasting heat waves in the 21st century. *Science*, 305(5686):994–997, 2004.

[2] Stefan Rahmstorf and Dim Coumou. Increase of extreme events in a warming world. *Proceedings of the National Academy of Sciences*, 108(44):17905–17909, 2011.

[3] EM Fischer, Sebastian Sippel, and Reto Knutti. Increasing probability of record-shattering climate extremes. *Nature Climate Change*, 11(8):689–695, 2021.

[4] Noah S Diffenbaugh, Deepti Singh, Justin S Mankin, Daniel E Horton, Daniel L Swain, Danielle Touma, Allison Charland, Yunjie Liu, Matz Haugen, Michael Tsiang, et al. Quantifying the influence of global warming on unprecedented extreme climate events. *Proceedings of the National Academy of Sciences*, 114(19):4881–4886, 2017.

[5] Kristie L Ebi, Anthony Capon, Peter Berry, Carolyn Broderick, Richard de Dear, George Havenith, Yasushi Honda, R Sari Kovats, Wei Ma, Arunima Malik, et al. Hot weather and heat extremes: health risks. *The Lancet*, 398(10301):698–708, 2021.

[6] Daniela IV Domeisen, Elfatih AB Eltahir, Erich M Fischer, Reto Knutti, Sarah E Perkins-Kirkpatrick, Christoph Schär, Sonia I Seneviratne, Antje Weisheimer, and Heini Wernli. Prediction and projection of heatwaves. *Nature Reviews Earth & Environment*, 4(1):36–50, 2023.

[7] Jean-Marie Robine, Siu Lan K Cheung, Sophie Le Roy, Herman Van Oyen, Clare Griffiths, Jean-Pierre Michel, and François Richard Herrmann. Death toll exceeded 70,000 in europe during the summer of 2003. *Comptes Rendus. Biologies*, 331(2):171–178, 2008.

[8] Sarah Perkins-Kirkpatrick, David Barriopedro, Roshan Jha, Lin Wang, Arpita Mondal, Renata Libonati, and Kai Kornhuber. Extreme terrestrial heat in 2023. *Nature Reviews Earth & Environment*, 5(4):244–246, 2024.

[9] Seung-Ki Min. Human influence can explain the widespread exceptional warmth in 2023. *Communications Earth & Environment*, 5(1):215, 2024.

[10] Solomon Hsiang, Robert Kopp, Amir Jina, James Rising, Michael Delgado, Shashank Mohan, DJ Rasmussen, Robert Muir-Wood, Paul Wilson, Michael Oppenheimer, et al. Estimating economic damage from climate change in the united states. *Science*, 356(6345):1362–1369, 2017.

[11] Tamma Carleton, Amir Jina, Michael Delgado, Michael Greenstone, Trevor Houser, Solomon Hsiang, Andrew Hultgren, Robert E Kopp, Kelly E McCusker, Ishan Nath, et al. Valuing the global mortality consequences of climate change accounting for adaptation costs and benefits. *The Quarterly Journal of Economics*, 137(4):2037–2105, 2022.

[12] Olivier Deschênes and Michael Greenstone. Climate change, mortality, and adaptation: Evidence from annual fluctuations in weather in the US. *American Economic Journal: Applied Economics*, 3(4):152–85, 2011.

[13] Antonio Gasparrini, Yuming Guo, Francesco Sera, Ana Maria Vicedo-Cabrera, Veronika Huber, Shilu Tong, Micheline de Sousa Zanotti Stagliorio Coelho, Paulo Hilario Nascimento Saldiva, Eric Lavigne, Patricia Matus Correa, et al. Projections of temperature-related excess mortality under climate change scenarios. *The Lancet Planetary Health*, 1(9):e360–e367, 2017.

[14] Ana Maria Vicedo-Cabrera, Yuming Guo, Francesco Sera, Veronika Huber, Carl-Friedrich Schleussner, Dann Mitchell, Shilu Tong, Micheline de Sousa Zanotti Stagliorio Coelho, Paulo Hilario Nascimento Saldiva, Eric Lavigne, et al. Temperature-related mortality impacts under and beyond paris agreement climate change scenarios. *Climatic Change*, 150:391–402, 2018.

[15] David García-León, Pierre Masselot, Malcolm N Mistry, Antonio Gasparrini, Corrado Motta, Luc Feyen, and Juan-Carlos Ciscar. Temperature-related mortality burden and projected change in 1368 european regions: a modelling study. *The Lancet Public Health*, 9(9):e644–e653, 2024.

[16] Lisa Patel, Kathryn C Conlon, Cecilia Sorensen, Samia McEachin, Kari Nadeau, Khyati Kakkad, and Kenneth W Kizer. Climate change and extreme heat events: how health systems should prepare. *NEJM Catalyst Innovations in Care Delivery*, 3(7):CAT–21, 2022.

[17] Kristie L Ebi, Peter Berry, Katie Hayes, Christopher Boyer, Samuel Sellers, Paddy M Enright, and Jeremy J Hess. Stress testing the capacity of health systems to manage climate change-

related shocks and stresses. *International Journal of Environmental Research and Public Health*, 15(11):2370, 2018.

[18] Claudia Gessner, Erich M Fischer, Urs Beyerle, and Reto Knutti. Very rare heat extremes: quantifying and understanding using ensemble reinitialization. *Journal of Climate*, 34(16): 6619–6634, 2021.

[19] Samuel Lüthi, Christopher Fairless, Erich M Fischer, Noah Scovronick, Ben Armstrong, Micheline De Sousa Zanotti Stagliorio Coelho, Yue Leon Guo, Yuming Guo, Yasushi Honda, Veronika Huber, et al. Rapid increase in the risk of heat-related mortality. *Nature Communications*, 14(1):4894, 2023.

[20] Erich M Fischer, U Beyerle, L Bloin-Wibe, C Gessner, V Humphrey, F Lehner, AG Pendergrass, S Sippel, J Zeder, and R Knutti. Storylines for unprecedented heatwaves based on ensemble boosting. *Nature Communications*, 14(1):4643, 2023.

[21] Daniel E Horton, Nathaniel C Johnson, Deepti Singh, Daniel L Swain, Bala Rajaratnam, and Noah S Diffenbaugh. Contribution of changes in atmospheric circulation patterns to extreme temperature trends. *Nature*, 522(7557):465, 2015.

[22] Efi Rousi, Kai Kornhuber, Goratz Beobide-Arsuaga, Fei Luo, and Dim Coumou. Accelerated western european heatwave trends linked to more-persistent double jets over eurasia. *Nature Communications*, 13(1):3851, 2022.

[23] Jitendra Singh, Sebastian Sippel, and Erich M Fischer. Circulation dampened heat extremes intensification over the midwest usa and amplified over western europe. *Communications Earth & Environment*, 4(1):432, 2023.

[24] Robert Vautard, Julien Cattiaux, Tamara Happé, Jitendra Singh, Rémy Bonnet, Christophe Cassou, Dim Coumou, Fabio D'andrea, Davide Faranda, Erich Fischer, et al. Heat extremes in western europe increasing faster than simulated due to atmospheric circulation trends. *Nature Communications*, 14(1):6803, 2023.

[25] Kai Kornhuber, Samuel Bartusek, Richard Seager, Hans Joachim Schellnhuber, and Mingfang Ting. Global emergence of regional heatwave hotspots outpaces climate model simulations. *Proceedings of the National Academy of Sciences*, 121(49):e2411258121, 2024.

[26] Matthew Patterson. North-West Europe hottest days are warming twice as fast as mean summer days. *Geophysical Research Letters*, 50(10):e2023GL102757, 2023.

[27] Theodore G Shepherd, Emily Boyd, Raphael A Calel, Sandra C Chapman, Suraje Dessai, Ioana M Dima-West, Hayley J Fowler, Rachel James, Douglas Maraun, Olivia Martius, et al. Storylines: an alternative approach to representing uncertainty in physical aspects of climate change. *Climatic Change*, 151:555–571, 2018.

[28] Rowan T Sutton. Climate science needs to take risk assessment much more seriously. *Bulletin of the American Meteorological Society*, 100(9):1637–1642, 2019.

[29] Timo Kelder, Dorothy Heinrich, Lisette Klok, Vikki Thompson, Henrique MD Goulart, Ed Hawkins, Louise J Slater, Laura Suarez-Gutierrez, Robert L Wilby, Erin Coughlan de Perez, et al. How to stop being surprised by unprecedented weather. *Nature Communications*, 16(1):2382, 2025.

[30] Jana Sillmann, Theodore G Shepherd, Bart Van Den Hurk, Wilco Hazeleger, Olivia Martius, Julia Slingo, and Jakob Zscheischler. Event-based storylines to address climate risk. *Earth's Future*, 9(2):e2020EF001783, 2021.

[31] Anne Fouillet, Grégoire Rey, Vérène Wagner, Karine Laaidi, Pascal Empereur-Bissonnet, Alain Le Tertre, Philippe Frayssinet, Pierre Bessemoulin, Françoise Laurent, Perrine De Crouy-Chanel, et al. Has the impact of heat waves on mortality changed in France since the European heat wave of summer 2003? A study of the 2006 heat wave. *International Journal of Epidemiology*, 37(2):309–317, 2008.

[32] Erich M Fischer, Sonia I Seneviratne, Daniel Lüthi, and Christoph Schär. Contribution of land-atmosphere coupling to recent European summer heat waves. *Geophysical Research Letters*, 34(6), 2007.

[33] Diego G Miralles, Adriaan J Teuling, Chiel C Van Heerwaarden, and Jordi Vila-Guerau De Arellano. Mega-heatwave temperatures due to combined soil desiccation and atmospheric heat accumulation. *Nature Geoscience*, 7(5):345–349, 2014.

[34] Abderrezak Bouchama and James P Knochel. Heat stroke. *New England Journal of Medicine*, 346(25):1978–1988, 2002.

[35] Joan Ballester, Marcos Quijal-Zamorano, Raúl Fernando Méndez Turrubiates, Ferran Pegenaute, François R Herrmann, Jean Marie Robine, Xavier Basagaña, Cathryn Tonne, Josep M Antó, and Hicham Achebak. Heat-related mortality in Europe during the summer of 2022. *Nature medicine*, 29(7):1857–1866, 2023.

[36] Elisa Gallo, Marcos Quijal-Zamorano, Raúl Fernando Méndez Turrubiates, Cathryn Tonne, Xavier Basagaña, Hicham Achebak, and Joan Ballester. Heat-related mortality in Europe during 2023 and the role of adaptation in protecting health. *Nature Medicine*, pages 1–5, 2024.

[37] Thessa M Beck, Dominik L Schumacher, Hicham Achebak, Ana M Vicedo-Cabrera, Sonia I Seneviratne, and Joan Ballester. Mortality burden attributed to anthropogenic warming during Europe's 2022 record-breaking summer. *npj Climate and Atmospheric Science*, 7(1):245, 2024.

[38] Jared T Trok, Elizabeth A Barnes, Frances V Davenport, and Noah S Diffenbaugh. Machine learning–based extreme event attribution. *Science Advances*, 10(34):eadl3242, 2024.

[39] DM Smith, AA Scaife, E Hawkins, Roberto Bilbao, GJ Boer, Mihaela Caian, L-P Caron, G Danabasoglu, T Delworth, Francisco J Doblas-Reyes, et al. Predicted chance that global warming will temporarily exceed 1.5 c. *Geophysical Research Letters*, 45(21):11–895, 2018.

[40] Noah S Diffenbaugh and Elizabeth A Barnes. Data-driven predictions of peak warming under rapid decarbonization. *Geophysical Research Letters*, 51(23):e2024GL111832, 2024.

[41] Daniel Mitchell, Clare Heaviside, Sotiris Vardoulakis, Chris Huntingford, Giacomo Masato, Benoit P Guillod, Peter Frumhoff, Andy Bowery, David Wallom, and Myles Allen. Attributing human mortality during extreme heat waves to anthropogenic climate change. *Environmental Research Letters*, 11(7):074006, 2016.

[42] C3S. The year 2024 set to end up as the warmest on record. *Copernicus Monthly Climate Bulletin*, 2024.

[43] Kai Chen, Evan De Schrijver, Sidharth Sivaraj, Francesco Sera, Noah Scovronick, Leiwen Jiang, Dominic Roye, Eric Lavigne, Jan Kyselỳ, Aleš Urban, et al. Impact of population aging on future temperature-related mortality at different global warming levels. *Nature communications*, 15(1):1796, 2024.

[44] Richard A Betts, Stephen E Belcher, Leon Hermanson, Albert Klein Tank, Jason A Lowe, Chris D Jones, Colin P Morice, Nick A Rayner, Adam A Scaife, and Peter A Stott. Approaching 1.5° C: how will we know we've reached this crucial warming mark? *Nature*, 624 (7990):33–35, 2023.

[45] Christopher W Callahan, Jared Trok, Andrew Wilson, Carlos Gould, Sam Heft-Neal, Marshall Burke, and Noah S Diffenbaugh. Quantifying the contributions of climate change and adaptation to mortality from unprecedented extreme heat events. *in review; preprint at https://eartharxiv.org/repository/dashboard/8573/*, 2025.

[46] Martin-Immanuel Bittner, Eva Franziska Matthies, Dafina Dalbokova, and Bettina Menne. Are european countries prepared for the next big heat-wave? *The European Journal of Public Health*, 24(4):615–619, 2014.

[47] Richard C Keller. *Fatal isolation: The devastating Paris heat wave of 2003*. University of Chicago Press, 2015.

[48] Marshall Burke, Mustafa Zahid, Mariana CM Martins, Christopher W Callahan, Richard Lee, Tumenkhusel Avirmed, Sam Heft-Neal, Mathew Kiang, Solomon M Hsiang, and David Lobell. Are we adapting to climate change? *National Bureau of Economic Research Working Paper*, 2024.

[49] Richard C Cornes, Gerard van der Schrier, Else JM van den Besselaar, and Philip D Jones. An ensemble version of the e-obs temperature and precipitation data sets. *Journal of Geophysical Research: Atmospheres*, 123(17):9391–9409, 2018.

[50] C3S. ERA5: Fifth generation of ECMWF atmospheric reanalysis of the global climate. *Copernicus Climate Change Service Climate Data Store*, 2017.

[51] Gerald A Meehl, Catherine A Senior, Veronika Eyring, Gregory Flato, Jean-Francois Lamarque, Ronald J Stouffer, Karl E Taylor, and Manuel Schlund. Context for interpreting equilibrium climate sensitivity and transient climate response from the CMIP6 Earth system models. *Science Advances*, 6(26):eaba1981, 2020.

[52] D. Chen, M. Rojas, B.H. Samset, K. Cobb, A. Diongue Niang, P. Edwards, S. Emori, S.H. Faria, E. Hawkins, P. Hope, P. Huybrechts, M. Meinshausen, S.K. Mustafa, G.-K. Plattner,

and A.-M. Tréguier. Framing, context, and methods. In V. Masson-Delmotte, P. Zhai, A. Pirani, S. L. Connors, C. Péan, S. Berger, N. Caud, Y. Chen, L. Goldfarb, M. I. Gomis, M. Huang, K. Leitzell, E. Lonnoy, J. B. R. Matthews, T. K. Maycock, T. Waterfield, O. Yelekçi, R. Yu, and B. Zhou, editors, *Climate Change 2021: The Physical Science Basis. Contribution of Working Group I to the Sixth Assessment Report of the Intergovernmental Panel on Climate Change*, chapter 1, pages 147–286. Cambridge University Press, Cambridge, UK and New York, NY, USA, 2021. doi: 10.1017/9781009157896.003.

[53] Olivier Deschenes and Enrico Moretti. Extreme weather events, mortality, and migration. *The Review of Economics and Statistics*, 91(4):659–681, 2009.

[54] Alan Barreca, Karen Clay, Olivier Deschenes, Michael Greenstone, and Joseph S Shapiro. Adapting to climate change: The remarkable decline in the US temperature-mortality relationship over the twentieth century. *Journal of Political Economy*, 124(1):105–159, 2016.

[55] Marshall Burke, Felipe González, Patrick Baylis, Sam Heft-Neal, Ceren Baysan, Sanjay Basu, and Solomon Hsiang. Higher temperatures increase suicide rates in the united states and mexico. *Nature climate change*, 8(8):723–729, 2018.

[56] Tamma A Carleton and Solomon M Hsiang. Social and economic impacts of climate. *Science*, 353(6304):aad9837, 2016.

[57] Tamma A Carleton. Crop-damaging temperatures increase suicide rates in India. *Proceedings of the National Academy of Sciences*, 114(33):8746–8751, 2017.

[58] Garth Heutel, Nolan H Miller, and David Molitor. Adaptation and the mortality effects of temperature across us climate regions. *The Review of Economics and Statistics*, 103(4):740–753, 2021.

[59] Solomon Hsiang. Climate econometrics. *Annual Review of Resource Economics*, 8:43–75, 2016.

[60] Antonio Gasparrini, Yuming Guo, Masahiro Hashizume, Eric Lavigne, Antonella Zanobetti, Joel Schwartz, Aurelio Tobias, Shilu Tong, Joacim Rocklöv, Bertil Forsberg, et al. Mortality risk attributable to high and low ambient temperature: a multicountry observational study. *The Lancet*, 386(9991):369–375, 2015.

[61] Ana Maria Vicedo-Cabrera, N Scovronick, Francesco Sera, Dominic Royé, Rochelle Schneider, Aurelio Tobias, Christofer Astrom, Y Guo, Y Honda, DM Hondula, et al. The burden of heat-related mortality attributable to recent human-induced climate change. *Nature Climate Change*, 11(6):492–500, 2021.

[62] J. Y. Lee, J. Marotzke, G. Bala, L. Cao, S. Corti, J. P. Dunne, F. Engelbrecht, E. Fischer, J. C. Fyfe, C. Jones, A. Maycock, J. Mutemi, O. Ndiaye, S. Panickal, and T. Zhou. Future global climate: Scenario-based projections and near-term information. In V. Masson-Delmotte, P. Zhai, A. Pirani, S. L. Connors, C. Péan, S. Berger, N. Caud, Y. Chen, L. Goldfarb, M. I. Gomis, M. Huang, K. Leitzell, E. Lonnoy, J. B. R. Matthews, T. K. Maycock, T. Waterfield, O. Yelekçi, R. Yu, and B. Zhou, editors, *Climate Change 2021: The Physical Science Basis. Contribution of Working Group I to the Sixth Assessment Report of the Intergovernmental Panel on Climate Change*, chapter 4. Cambridge University Press, Cambridge, United Kingdom and New York, NY, USA, 2021.

[63] Veronika Eyring, Sandrine Bony, Gerald A Meehl, Catherine A Senior, Bjorn Stevens, Ronald J Stouffer, and Karl E Taylor. Overview of the Coupled Model Intercomparison Project Phase 6 (CMIP6) experimental design and organization. *Geoscientific Model Development*, 9(5):1937–1958, 2016.

[64] Brian C O'Neill, Claudia Tebaldi, Detlef P van Vuuren, Veronika Eyring, Pierre Friedlingstein, George Hurtt, Reto Knutti, Elmar Kriegler, Jean-Francois Lamarque, Jason Lowe, et al. The Scenario Model Intercomparison Project (ScenarioMIP) for CMIP6. *Geoscientific Model Development*, 9(9):3461–3482, 2016.